



**Unimolecular Dissociation Dynamics of Electronically
Excited HCO(): Rotational Control of Nonadiabatic Decay**

Journal:	<i>Faraday Discussions</i>
Manuscript ID	FD-ART-01-2022-000011.R1
Article Type:	Paper
Date Submitted by the Author:	22-Feb-2022
Complete List of Authors:	Sun, Ge; University of California Riverside, Department of Chemistry Han, Shanyu; University of New Mexico College of Arts and Sciences Zheng, Xianfeng; Anhui Normal University Song, Yu; University of California Riverside Qin, Yuan; University of California Riverside Dawes, Richard; Missouri University of Science and Technology, Chemistry Xie, Daiqian; Nanjing University, Department of Chemistry Zhang, Jingsong; University of California Riverside Guo, Hua; University of New Mexico College of Arts and Sciences, Department of Chemistry

Submitted to Faraday Discussions, 1/18/2022, submitted 2/22/2022

**Unimolecular Dissociation Dynamics of Electronically Excited $\text{HCO}(\tilde{A}^2A'')$: Rotational
Control of Nonadiabatic Decay**

Ge Sun,^{a,#} Shanyu Han,^{b,#} Xianfeng Zheng,^{a,c} Yu Song,^a Yuan Qin,^a Richard Dawes,^d Daiqian
Xie,^e Jingsong Zhang^{a,*} and Hua Guo,^{b,*}

^a*Department of Chemistry, University of California Riverside, Riverside, CA 92521, USA*

^b*Department of Chemistry and Chemical Biology, University of New Mexico, Albuquerque, NM
87131, USA*

^c*Anhui Province Key Laboratory of Optoelectric Materials Science and Technology, Department
of Physics, Anhui Normal University, Wuhu, Anhui 241000, China*

^d*Department of Chemistry, Missouri University of Science and Technology, Rolla, MO 65409,
USA*

^e*Institute of Theoretical and Computational Chemistry, Key Laboratory of Mesoscopic
Chemistry, School of Chemistry and Chemical Engineering, Nanjing University, Nanjing 210093,
China*

#: these two authors contributed equally.

*: corresponding authors, emails: jszhang@ucr.edu, hguo@unm.edu

Abstract

The photoinduced unimolecular decay of the electronically excited $\text{HCO}(\tilde{A}^2A'')$ is investigated in a combined experimental-theoretical study. The molecule is excited to the $(1, n_2, 0)$ combination bands, which decay via Renner-Teller coupling to the ground electronic state. The rovibrational state distribution of the CO fragment was measured via the high- n Rydberg H-atom time-of-flight method and calculated using a wave packet method on an accurate set of potential energy surfaces. It is shown that the non-adiabatic decay rate is strongly modulated by the HCO rotational angular momentum, which leaves unique signatures in the product state distribution. The experimentally observed bimodal rotational distribution of the dominant $\text{CO}(v=0)$ fragment is likely due to decay of different vibronic states populated by the excitation and modulated by the excited state lifetime, which is in turn controlled by the parent rotational quantum number.

I. Introduction

In Lindemann's mechanism,¹ a unimolecular reaction on the ground electronic state occurs on a single Born-Oppenheimer potential energy surface (PES),² where the stable molecule, supported by a potential well, decomposes into fragments, driven by energy transfer with bath molecules. Statistical theories, such as that due to Rice, Ramsperger, Kassel and Marcus (RRKM), provide a generally accurate description of the decay rate, assuming energy randomization is complete in the potential well.¹ For those systems, dynamical effects are often negligible.

However, the decay of an electronically excited species often departs significantly from the statistical limit, because the excited state PES is likely to intersect those of lower states through electronic degeneracies, as realized by the pioneers of quantum mechanics nearly a hundred years ago.³⁻⁵ The coupling between different electronic states can be quite strong near these degeneracies, leading to facile nonadiabatic transitions to the lower electronic states.^{6, 7} Such scenarios break down the Born-Oppenheimer adiabatic approximation,² which neglects the coupling between different electronic states. It is now well established that nonadiabatic effects are prevalent in chemical systems, particularly when excited species are involved.⁸⁻¹³ Importantly, such transitions could lead to rapid fragmentation even under collision-free conditions,¹⁴⁻¹⁶ which violates the statistical assumption. Under such circumstances, dynamics becomes important and cannot be ignored.¹⁶

In this contribution, we examine a prototypical nonadiabatic unimolecular process, in which the electronically excited HCO molecule is prepared by optical pumping. Its subsequent decay to the ground electronic state via Renner-Teller (RT) coupling is followed by its dissociation into H and CO fragments. By measuring the H-atom product kinetic energy release, the CO rovibrational state distributions can be determined. The product state distribution carries rich information on the

nonadiabatic transition and subsequent dynamics, which is deciphered by full-dimensional quantum dynamics calculations on a set of ab initio PESs for this system.

The first absorption band of HCO has been extensively investigated. As the \tilde{A}^2A'' state of HCO has a linear equilibrium geometry, the excitation from the bent HCO(\tilde{X}^2A') results in a progression of pure bending states, denoted as $(0, n_2^K, 0)$, which dominate the absorption band.¹⁷ In addition, there are some other weaker combination bands, with excitations in either the C-H (n_1) and/or C-O (n_3) modes. All bands have diffuse structures, due apparently to predissociation via the RT coupling with the ground state. The lifetimes of these vibronic resonances were later measured¹⁸ and theoretically calculated.¹⁹ The RT effect, which is a type of nonadiabatic transition facilitated by the coupling of the electronic angular momentum with the rotational angular momentum of the molecule,²⁰ becomes dominant near the collinear geometry of HCO, where the \tilde{A}^2A'' and \tilde{X}^2A' states form the degenerate pair of the $^2\Pi$ state. Because of the nonadiabatic nature of the RT coupling, these predissociative features in HCO are also called vibronic resonances.

In a series of experiments by Houston and coworkers in the 1990s,²¹⁻²³ the CO product upon photodissociation of HCO in its \tilde{A} band was measured and found to be highly rotationally excited with an apparently oscillatory distribution. Subsequent theoretical work revealed that the rotational excitation in the CO product can be rationalized by the strong torque induced by the ground-state PES after the nonadiabatic transition from the excited state.^{24,25} The oscillation in the CO rotational distribution was established later using a higher-resolution experimental technique and attributed to interference between two different dissociation paths on the ground electronic state.²⁶

The highly structured absorption bands of HCO(\tilde{A}^2A'') offer a rare opportunity for understanding the mode specificity in unimolecular decay of an excited species. The excitation of

the C-O (n_3) mode was initially thought to have little impact on the CO product rotational distribution,²³ as it is well established that the CO moiety is a spectator during dissociation. However, in our recent publication,²⁷ it was demonstrated that the decay of the vibronic resonances $(0, n_2^K, 1)$ yielded CO products in its ground vibrational state, as well as in the $\nu=1$ state. Detailed analysis revealed that this seemingly contradictory observation stemmed from the fact that the $(0, n_2^K, 1)$ resonances borrow intensity from the nearby $(0, (n_2+2)^K, 0)$ ones, because the short lifetime rendered by the fast nonadiabatic decay with large ($J>0$) molecular rotational angular momenta results in a broad energy span according to Heisenberg's uncertainty principle, and thus the intensity borrowing. The non-zero rotational angular momentum ($J>0$) states needed to be included in the simulation because they have significant Boltzmann weights at the experimental temperature and they behave differently in nonadiabatic transitions. This surprising rotational modulation of the nonadiabatic dynamics presented a unique case where quantum effects dominate the dynamics.

Another interesting observation in state-specific decay of HCO(\tilde{A}^2A'') is that the excitation of C-H (n_1) mode appears to enhance the rotational excitation of CO products.²³ In addition, dissociation of the $(1, n_2^K, 0)$ states leads to a bimodal CO rotational distribution. For example, dissociation of the $(1, 9^0, 0)$ state shifts the main peak from $j=27$ for the $(0, 9^0, 0)$ state to $j=45$, but it also possesses a second and weaker peak at $j=22$.²³ Similarly, measurements reported in this work on the dissociation of the $(1, 8^1, 0)$ state reveal a main peak at $j=39$ and second peak near $j=30$ (see below). This bimodality was initially attributed by Goldfield *et al.* to the node in the $(1, n_2^K, 0)$ wave function,²⁴ which is reflected to the CO rotational distribution. However, positions of the peaks in the two-dimensional theoretical study by these authors did not agree with experiment, making the explanation less convincing. Schinke and coworkers²⁵ also observed weak bimodality for $(1, 10^1, 0)$ in their theoretical work with all dimensions included, which correctly obtained the

peak positions but underestimated the intensity at the peak of $j=30$. Unfortunately, they did not explain the origin of the bimodality.

In this contribution, we perform a joint experimental-theoretical study on the unimolecular decay dynamics of the $(1, n_2^K, 0)$ vibronic resonances of $\text{HCO}(\tilde{A}^2A'')$. The experiment measured the kinetic energy release of the H co-fragment, upon laser excitation to each resonance state. The bimodality was confirmed in our new experiment. To simulate the experiment, we carried out full-dimensional wave packet dynamics calculations on a set of diabatic PESs based on high level *ab initio* points. These calculations clearly refute the earlier suggestion that the two peaks in the bimodal CO rotational distribution are due to the nodal structure of the excited state wavefunction. Instead, we attribute the lower peak around $j=30$ to the intensity borrowing from a nearby pure bending state $(0, n_2, 0)$, via a similar mechanism proposed in our most recent work.²⁷ Furthermore, we show that the intensity of this peak is controlled by the overall rotation of the parent molecule. We conclude that the bimodality observed in the experiment is instead a consequence of the average over different initial rotational states of the parent molecule at the experimental temperature, which underscores the complexity of the nonadiabatic dynamics in this seemingly simple system. This work is organized as follows. Section II briefly introduces the experimental apparatus and theoretical method. The results are presented and discussed in Section III. The conclusion is given in Section IV.

II. Methods

A. Experiment

The high- n Rydberg H-atom time-of-flight (HRTOF) technique and experimental apparatus have been reported in previous publications,²⁸⁻³⁰ so only a very brief summary is given here. Acrolein (> 95%, Fluka) was used as the precursor for the HCO radical in this work. The HCO

radicals were generated by photolyzing the precursor in Ar ($\sim 2\%$ concentration with a total pressure of 120 kPa) with the 193 nm radiation of an ArF excimer laser in front of the pulsed nozzle. The HCO radicals produced from the photolysis were entrained in the seeded molecular beam and subsequently cooled by supersonic expansion. The HCO molecular beam was collimated at 2.8 cm downstream by a 1 mm diameter skimmer into a high-vacuum chamber. In the reaction chamber, 4.6 cm downstream of the skimmer, the HCO radicals were photoexcited by a slightly focused laser beam (in the region of 490 to 715 nm, line width $\sim 0.2 \text{ cm}^{-1}$, and focal length of the lens $\sim 100 \text{ cm}$). The photolysis radiation was tuned to the HCO(\tilde{A}^2A'') vibronic resonances, and the wavelength of the photolysis laser was monitored by a wavemeter (Burleigh WA-4500). A Fresnel-Rhomb achromatic $\lambda/2$ plate was used to change the polarization of the photolysis radiation for the product angular distribution measurements. The H-atoms produced from the photodissociation of HCO were pumped by two-color resonant excitation (121.6 nm + 366.2 nm), i.e., from 1^2S to 2^2P via the H-atom Lyman- α transition then further to a metastable high- n Rydberg state. A small portion of the high- n Rydberg state H-atoms drifted with their nascent velocities to a microchannel plate (MCP) detector which was positioned perpendicular to the molecular beam and were field ionized in front of the detector and detected. The nominal flight distance was 37.10 cm, which was calibrated by photodissociation of HBr at 236 nm with the well-studied HBr bond dissociation energy and the spin-orbit energy of the $\text{Br}(^2P_{3/2})$ and $\text{Br}(^2P_{1/2})$ products. The H-atom TOF spectra were accumulated from $\sim 200\text{k}$ laser shots for each spectrum. By characterizing the (1+1) resonance enhanced multiphoton ionization (REMPI) spectra of the HCO $\tilde{B}^2A' \leftarrow \tilde{X}^2A'$ transition, the rotational temperature of the HCO radicals in the molecular beam was estimated to be $\sim 20\text{K}$.

The H-atom TOF spectra of photodissociation of the HCO were obtained in the region of 490 to 715 nm. The polarization of the photolysis radiation was set parallel (\parallel , $\theta = 0^\circ$) and perpendicular (\perp , $\theta = 90^\circ$) to the TOF path. The net H-atom product TOF spectra were obtained by removing the precursor background spectra.

The center-of-mass (CM) translational energy distributions of the H + CO products, $P(E_T)$, can be calculated from the H-atom product TOF spectra with the following expression:

$$E_T = \left(1 + \frac{m_H}{m_{CO}}\right) E_H + \frac{m_H}{m_{CO}} E_{HCO} = \frac{1}{2} m_H \left(1 + \frac{m_H}{m_{CO}}\right) \left(\frac{L}{t_H}\right)^2 + \frac{m_H}{m_{CO}} E_{HCO}, \quad (1)$$

in which E_H and E_{HCO} are the laboratory translation energy of the H-atom product and the HCO radical, L is the flight length of the TOF, and t_H is the flight time of the H-atom product. The second term is due to the motion of the parent HCO radical in the molecular beam, which was perpendicular to the TOF path, and based on the beam velocity of ~ 580 m/s for the HCO/Ar gas mixture, the term is estimated to be about 15 cm^{-1} .

The CM product translational energy dependent and the photofragment angular distribution is described in the following equation:³¹

$$P(E_T, \theta) = \left(\frac{1}{4\pi}\right) P(E_T) [1 + \beta P_2(\cos\theta)], \quad (2)$$

where β is the anisotropy parameter ($-1 \leq \beta \leq 2$), θ is the angle between the electric vector of the linear polarized photolysis radiation and the recoiling velocity of the H-atom product, $P(E_T)$ is the angle integrated CM translational energy distributions, and the $P_2(\cos\theta)$ is the second-order Legendre polynomial. The energy dependent anisotropy parameter, $\beta(E_T)$ can be derived from the product translational energy distribution with the photolysis parallel and perpendicular to the TOF axis, with $\beta(E_T) = 2 \times [P_{\parallel}(E_T) - P_{\perp}(E_T)] / [P_{\parallel}(E_T) + 2P_{\perp}(E_T)]$. Since the β parameters essentially stay

constant for the photodissociation of the HCO(\tilde{A}^2A'') ($0, 9^0, 0$), ($0, 10^1, 0$), and ($0, 12^1, 0$) states,²⁶ then the β parameter can be expected to stay nearly constant in the photodissociation of other vibrational levels of the HCO(\tilde{A}^2A'') state.

B. Theory

The Renner-Teller (RT) effect is a non-Born-Oppenheimer phenomenon facilitated by the coupling between the projection of the total rotational angular momentum onto the molecular axis (K) and the projection of the electronic orbital angular momentum on to the same axis (Λ).²⁰ Following the treatment of Petrongolo³² and Goldfield,²⁴ the nonadiabatic Hamiltonian in the Jacobi coordinates (r, R, γ) is given for HCO ($\hbar=1$ hereafter):

$$\hat{H} = -\frac{1}{2\mu_R} \frac{\partial^2}{\partial R^2} - \frac{1}{2\mu_r} \frac{\partial^2}{\partial r^2} + \hat{T}_{rot} + \hat{H}_{el}, \quad (3)$$

where μ_R and μ_r are the reduced masses for R (H-CO distance) and r (CO distance), respectively.

The electronic Hamiltonian is given by \hat{H}_{el} , the eigenvalues of which are the PESs. The rotational kinetic energy operator is written as

$$\begin{aligned} \hat{T}_{rot} = & (B_R + b_r) \left[-\frac{1}{\sin \gamma} \frac{\partial}{\partial \gamma} \sin \gamma \frac{\partial}{\partial \gamma} + \frac{\hat{N}_z^2}{\sin^2 \gamma} \right] + B_R \left[\hat{J}^2 - 2\hat{J}_z^2 - \hat{L}_z^2 \right. \\ & \left. + 2\hat{J}_z \hat{L}_z + \hat{J}_+ \left(\cot \gamma \hat{N}_z + \frac{\partial}{\partial \gamma} \right) + \hat{J}_- \left(\cot \gamma \hat{N}_z - \frac{\partial}{\partial \gamma} \right) \right], \end{aligned} \quad (4)$$

where $B_R = \frac{1}{2\mu_R R^2}$ and $b_r = \frac{1}{2\mu_r r^2}$. The body-fixed (BF) frame is defined with its Z -axis along the R vector (R -embedding). Ignoring the electronic spin, the nuclear angular momentum operator (\hat{N}) is given by the difference between the total (\hat{J}) and electronic orbital (\hat{L}) angular momenta:

$\hat{N} = \hat{J} - \hat{L}$, and $\hat{L} \approx \hat{L}_z$. The X and Y components of the electronic orbital angular momentum are typically small and thus ignored, simplifying the Hamiltonian. The coupling of the nuclear and electronic properties suggest the breakdown of the Born-Oppenheimer approximation.

The calculations were performed in a diabatic electronic representation, defined by the eigenfunctions $|\lambda\rangle$ of the electronic angular momentum operator ($\hat{L}_z|\lambda\rangle = \lambda|\lambda\rangle$) with $\lambda = \pm 1$ for the Π state of linear HCO. This quantization of \hat{L}_z for the linear molecule is assumed to be held even at non-linear geometries. The ground and excited adiabatic electronic states of HCO are thus linear combinations of the two diabatic states. The details of the electronic structure calculations and fitting of the PESs can be found in Ref. 33. For details of the implementation of the Hamiltonian for triatomic systems, the reader is referred to Refs. 19, 25, 34.

The initial wave packet is chosen as follows:

$$\Psi_0 = \sum_{J=J_i-1}^{J_i+1} (-1)^{M_i} \begin{pmatrix} 1 & J_i & J \\ 0 & M_i & -M_i \end{pmatrix} \sum_{\Omega=\lambda}^J \psi^{J\Omega p}(r, R, \gamma) |J, \Omega, M_i, p\rangle, \quad (5)$$

with

$$\begin{aligned} \psi^{J\Omega p}(r, R, \gamma) = & \sqrt{(2J+1)(2J_i+1)} \delta_{p, p_i+1} \sum_{\Omega_i=\lambda_i}^{J_i} \psi^{J_i \Omega_i p_i}(r, R, \gamma, E_i) (-1)^{\Omega_i} \\ & \times \left\{ \frac{\mu_y}{\sqrt{2}} \left[\begin{pmatrix} 1 & J_i & J \\ 1 & \Omega_i & -1-\Omega_i \end{pmatrix} \delta_{\Omega, \Omega_i+1} (1-\delta_{0, \Omega_i}) - \right. \right. \\ & \left. \left. \sqrt{(1+\delta_{0, \Omega_i-1})} \begin{pmatrix} 1 & J_i & J \\ -1 & \Omega_i & 1-\Omega_i \end{pmatrix} \delta_{\Omega, \Omega_i-1} (1-\delta_{0, \Omega_i}) \right] \right\}, \quad (6) \end{aligned}$$

Here, J_i is the total angular momentum of HCO(\tilde{X}^2A') and its projection on the BF axis is defined by Ω_i . The wavefunction $\psi^{J_i \Omega_i p_i}(r, R, \gamma, E_i)$ is obtained on the ground state PES using the

iterative Lanczos algorithm.³⁵ p_i is the parity and M_i is the projection of J_i onto the z-axis of the space-fixed (SF) frame, in which the molecule is placed on the x - z plane. The selection rules for the $\tilde{A}^2 A'' \leftarrow \tilde{X}^2 A'$ transition dictate that the only non-zero transition dipole moment is in the y direction (μ_y), which has been calculated and fitted in our earlier work.²⁷

The wave packet was propagated using the Chebyshev evolution operator,^{36, 37} and the absorption spectrum and product distributions were obtained by the cosine Fourier transform of the auto- or cross-correlation functions, respectively.^{38, 39} We emphasize that the Coriolis coupling was fully included in our calculations, which is important for nonadiabatic transitions, as discussed below. The numerical parameters are given in Table I.

As shown in our previous work on this system,^{26, 27} several low-lying rotational states of HCO($\tilde{X}^2 A'$) have significant Boltzmann populations at the experimental temperature (20 K), and their contributions to the dissociation dynamics are quite different. Consequently, they should be included in the simulation. The rotational states of ground state HCO, which is an asymmetric rotor, are labeled by $J_{iK_{ai}K_{ci}}$, where K_{ai} and K_{ci} are the projections of J_i on the a and c rotational axes, respectively. In this work, six $K_{ai} = 0$ initial rotational states, namely 0_{00} , 1_{01} , 2_{02} , 3_{03} , 4_{04} , 5_{05} , and eight $K_{ai} = 1$ states, 1_{10} , 1_{11} , 2_{11} , 2_{12} , 3_{12} , 3_{13} , 4_{14} , 4_{13} , were chosen in the study of $(1, 10^1, 0)$ and $(1, 9^0, 0)$ dissociation, respectively. Here, the values of K_{ai} , which is approximately the same as K because of the light mass of H, were chosen because of the selection rule $\Delta K = \pm 1$. These states were selected based on their large Boltzmann weights. In the experiment, the photolysis photon wavelength was centered on the Q branch. For $(1, 9^0, 0)$, the linewidth was only around 0.2 cm^{-1} exhibiting a sharp peak in the action spectra, so only $\Delta J = 0$ transitions were included in the calculation. For $(1, 10^1, 0)$, on the other hand, the P , Q , and R branches significantly

overlapped due to the broad linewidths. Thus, $\Delta J = 0, \pm 1$ transitions were all included for the average.

III. Results and Discussion

The measured CM product translational energy distribution from the photodissociation of the $\text{HCO}(\tilde{A}^2A'') (1, 9^0, 0)$ state to the $\text{H} + \text{CO}$ products is shown in Figure 1. The position of the ground state $\text{CO} (\nu=0, j=0)$ product is indicated by an arrow in the figure. By deconvoluting the measured CO product internal energy distributions with Gaussian peaks, the CO product rotational state distribution can be obtained (see more in Supporting information, SI). The fitting process was not unique as many of the peaks belonging to different CO vibrational manifolds overlap. Nevertheless, the possible range and a best estimate of the relative populations of the $\text{CO} \nu=0$ and $\nu=1$ products can be assessed by comparing the quality of the simulated and measured CO internal energy distributions. Furthermore, due to the relatively small contributions of the $\text{CO} \nu=1$ state product, it was found that the uncertainty in the fitting process had little impact on the fitting quality for the $\nu=0$ rotational state distributions. The resulting CO product internal energy distributions from the photodissociation of the $\text{HCO}(\tilde{A}^2A'') (1, 9^0, 0)$ state and the fitting for the CO rovibrational state distributions are presented in Figure 2. (For all other resonance states, the data are provided in Figure S1-S7 in SI.) Likewise, the CO rovibrational state distributions of the $(1, 10^1, 0)$ and $(1, 8^1, 0)$ states were also obtained, which are displayed in Figure 3. In the same figure, the theoretical results are presented for comparison, in which the calculated photon wavelengths of the $(1, 8^1, 0)$, $(1, 9^0, 0)$, and $(1, 10^1, 0)$ states are 18728, 19507, 20201 cm^{-1} , compared to the measured values of 18676, 19403, and 20136 cm^{-1} (More comparisons of the calculated and measured excitation energies can be found in our previous work.^{26, 27}) The shifts in

the excitation energy are all on the order of 100 cm^{-1} , and they are due to the residual inaccuracies in the PESs.

Because the HRTOF technique measured the H-atom product, providing a uniform detection sensitivity of the co-fragment CO in different rovibrational levels, and the CO vibrational distributions were constrained in the fitting of the experimental CM product translational energy distributions, the agreement between theoretical and experimental vibrational distributions is quite good. The population of the $v=1$ state of the CO product can be attributed to the intensity borrowing of the nearby $(0, (n_2+2)^K, 1)$ states, as discussed extensively in our earlier work.²⁷

The bimodal feature in the experimental rotational product distributions of $\text{CO}(v=0)$ are clearly observable in all three vibronic resonances studied here, which confirms the earlier report by Houston and coworkers for the $(1, 9^0, 0)$ state.²³ The main peak is at around $j=40$ (denoted as Peak I in the following discussion), while the secondary peaks (denoted as Peak II below) at around $j=32$ for the three resonance states are very pronounced. The corresponding ratio is $P(j=31) : P(j=43) = 1 : 1.29$ for the $(1, 10^1, 0)$ state. Peak II is quite similar to the main peak for dissociation from the pure bending $(0, n_2^K, 0)$ states dominating the A band of HCO.²⁶

Unlike several previous theoretical studies,^{24,25} the calculated $\text{CO}(v=0)$ rotational distributions in Figure 3 were averaged over several low-lying rotational states of $\text{HCO}(\tilde{X}^2A')$. The Boltzmann weights at the experimental temperature of 20 K are given in SI. This Boltzmann average represents a more faithful simulation of the experimental conditions, as we emphasized in our recent work^{26,27} and show below. While the Boltzmann weighted rotational distributions are in overall agreement with experiment, the bimodality is not as pronounced in these calculation results. In particular, there is neither obvious Peak II at small j values nor the trough between the two peaks. Previous theoretical work by Schinke *et al.*²⁵ did observe weak bimodality for $(1, 10^1, 0)$ but the

intensity at Peak II was underestimated, with a ratio $P(j=30) : P(j=45) = 1 : 3$. Although those authors stated that the bimodal distribution was a result of averaging, they provided no detail on how the averaging was done (in Figure 13 of Ref. 25). Goldfield *et al.*²⁴ interpreted the double peaks as the reflection of the nodal structure in the excited state wave function along the C-H coordinate, but the two peaks are both near high $j \sim 40$ states. We have also observed two peaks in our single transition ($J=1 \leftarrow J_i=0$) calculations that are similar to those in the previous work,²⁴ as shown in Figure S8 in SI. These two peaks are the result of the nodal structure in the initial wavefunction, as pointed out by Goldfield *et al.*,²⁴ but both below to Peak I as there is almost no population for $j < 30$.

Here, we propose that the bimodality is due to the CO($v=0$) rotational distributions from different parent rotational quantum numbers (J_i). To illustrate this point, we have included in Figure 3 the CO($v=0$) rotational distributions resulted from individual transitions from several low-lying J_i states, all with large Boltzmann weights. For transitions from low J_i states, the peak position of the CO rotational distribution more or less coincides with Peak I. For transitions from higher J_i states, on the other hand, the peak position shifts to lower j values. In the $(1, 9^1, 0)$ case, for example, the $J = 1 \leftarrow J_i = 1$ and $J = 2 \leftarrow J_i = 2$ distributions both peak at $j=42$, while the $J = 3 \leftarrow J_i = 3$ and $J = 4 \leftarrow J_i = 4$ distributions peak at $j=32$ and 34 , respectively. These parent rotational state-specific results clearly point to a strong rotational control of the dissociation dynamics. If we consider the dominant transitions at the experimental temperature and average them according to the corresponding Boltzmann factors ($(2J_i + 1)e^{-E_{J_i}/kT}$), the resultant ratio for the two peaks agrees better with the experimental value than only the single transition, even when the bimodality is not clear.

The mechanism identified here is the same as what we proposed in our previous work on the rotational modulation of the CO vibrational distribution upon photodissociation from the $(0, n_2, 1)$ states.²⁷ For our discussion here, we focus on the $(1, 10^1, 0)$ state. As shown in Figure 4, this resonance is energetically close to two other vibronic resonances $(0, 14^1, 0)$ and $(0, 12^1, 1)$. For excitation to a low J value, the projection onto the collinear HCO axis (Ω) is necessarily small ($\Omega \leq J$). If this projection is small, coupling with the electronic angular momentum will also be small, and, as a result, the lifetime of the excited state is long. On the other hand, the excitation to a higher J state opens up high Ω channels via the Coriolis coupling, which leads to a short lifetime due to increased RT coupling. This is clearly shown in the Figure 4 where the autocorrelation function and the spectrum are plotted for several individual transitions.

For a short-lived excited state prepared at a high J value, exemplified by the $J=4 \leftarrow J_i=3$ transition, its state has necessarily a large energy width, following Heisenberg's uncertainty principle. Consequently, it contains excitation not just to the intended $(1, 10^1, 0)$ state, but also the nearby $(0, 14^1, 0)$ and $(0, 12^1, 1)$ states, as shown by the spectra in Figure 4. In fact, the $(0, 14^1, 0)$ state has the largest intensity, thanks to its large Franck-Condon factor. Consequently, the CO product rotational distribution is dominated by dissociation from the $(0, 14^1, 0)$ state via intensity borrowing, which leads to the colder rotational products at Peak II, as shown in Figure 3. The oscillation in the rotational distributions is, as discussed in our earlier work,²⁶ due to interference on the ground electronic state of HCO.

For a long-lived excited state prepared at a low J value, such as the $J=1 \leftarrow J_i=0$ transition, the wave function on the excited state is essentially the eigenstate of $(1, 10^1, 0)$, resulting in the highly inverted rotational distribution of the products at Peak I. The enhancement of the rotational excitation in the CO product by the excitation of the C-H vibration is known and attributable to

the access of regions of the ground state PES that have stronger anisotropy, which exerts a larger torque on the incipient CO (Figure S9).^{23,25} The evolution of the excited state wave packet, which is shown in Figure 5 at different times after the initial excitation, shows clearly an initial appearance of the $(0, 14^1, 0)$ character due to the larger Franck-Condon factor than that of the $(1, 10^1, 0)$ state, culminating with the $(1, 10^1, 0)$ eigenstate in the long-time limit. These time-dependent wave packets were obtained by assembling the Chebyshev wave packets.⁴⁰

Although the overall agreement between the measured and calculated $\text{CO}(v=0)$ rotational state distributions is quite satisfactory, the absence of the bimodality in the latter is somewhat disappointing. There might be several reasons for the failure in reproducing the bimodal feature. One is the presence of small errors in the PESs, which are illustrated by the $\sim 100 \text{ cm}^{-1}$ differences between the calculated and measured vibronic band origins. Such minor errors might not be a large factor in conventional dynamics, but they could impact in a significant way the delicate balance between the excited state lifetime and energy gaps among the vibronic resonances.

IV. Conclusions

In this combined experimental-theoretical study, we provide detailed insights into the nonadiabatic predissociative dynamics of the $(1, n_2^K, 0)$ resonances of HCO in its first absorption band. Compared to those previous experimental studies, the new experiment was carried out using the HRTOF technique which affords a higher resolution and a uniform detection sensitivity. Our theoretical model involves multiple low-lying rotational states of $\text{HCO}(\tilde{X}^2A')$ present under experimental conditions and they lead to quite different product state distributions. The reason for the rotational modulation can be traced back to the lifetime of the excited state species, which is controlled by the Renner-Teller coupling. For low J states, the lifetime is sufficiently long that the intended $(1, n_2^K, 0)$ resonance is reached and the dissociation leads to highly excited rotational

states of CO. For higher J states, on the other hand, the lifetime is short and several nearby resonances $((0, (n_2+4)^K, 0)$ and $(0, (n_2+2)^K, 1)$ are simultaneously excited, which leads to both lower CO rotational excitation and population in CO($v=1$) state, respectively. The former is apparently responsible for the experimentally observed bimodality in the CO($v=0$) rotational distribution, even when the experimental distributions are not perfectly reproduced due to remaining errors in the potential energy surface. This study advanced our understanding of the rotational control of the Renner-Teller system, underscoring the quantum nature of the nonadiabatic dynamics.

Acknowledgments: This research was supported by the U.S. Department of Energy Office of Science, Office of Basic Energy Sciences (Grant Nos. DE-SC0015997 to H.G. and DE-SC0019740 to R.D.) and by the U.S. National Science Foundation (Grant No. CHE-1566636 to J.Z.). H.G. also acknowledges a Humboldt Research Award from the Alexander von Humboldt Foundation. We also thank partial support by the National Natural Science Foundation of China (Grant No. 21733006 to D.X.), the National Key Research and Development Program of China (Grant No. 2017YFA0206500 to D.X.), and University Cooperation and Innovation Program of Anhui Province (Grant No. GXXT 2020-004 to X.Z.). The calculations were performed at the Center for Advanced Research Computing (CARC) at UNM.

References

1. J. I. Steinfeld, J. S. Francisco and W. L. Hase, *Chemical Kinetics and Dynamics*, Prentice Hall, Englewood Cliffs, NJ, 1989.
2. M. Born and R. Oppenheimer, *Ann. Phys.*, 1927, **84**, 0457-0484.
3. J. von Neumann and E. Wigner, *Physik. Z.*, 1929, **30**, 467-470.
4. F. London, *Z. Phys.*, 1932, **74**, 143-174.
5. E. Teller, *J. Phys. Chem.*, 1937, **41**, 109-116.
6. M. Baer, *Beyond Born-Oppenheimer: Electronic Nonadiabatic Coupling Terms and Conical Intersections*, Wiley, New Jersey, 2006.
7. W. Domcke and D. R. Yarkony, *Annu. Rev. Phys. Chem.*, 2012, **63**, 325-352.
8. G. A. Worth and L. S. Cederbaum, *Annu. Rev. Phys. Chem.*, 2004, **55**, 127-158.
9. A. W. Jasper, S. Nangia, C. Zhu and D. G. Truhlar, *Acc. Chem. Res.*, 2006, **39**, 101-108.
10. B. G. Levine and T. J. Martínez, *Annu. Rev. Phys. Chem.*, 2007, **58**, 613-634.
11. M. S. Schuurman and A. Stolow, *Annu. Rev. Phys. Chem.*, 2018, **69**, 427-450.
12. J. Westermayr and P. Marquetand, *Chem. Rev.*, 2021, **121**, 9873-9926.
13. Y. Guan, C. Xie, D. R. Yarkony and H. Guo, *Phys. Chem. Chem. Phys.*, 2021, **23**, 24962-24983.
14. M. N. R. Ashfold and J. E. Baggott, *Molecular Photodissociation Dynamics*, The Royal Society of Chemistry, London, 1987.
15. L. J. Butler and D. M. Neumark, *J. Phys. Chem.*, 1996, **100**, 12801-12816.
16. R. Schinke, *Photodissociation Dynamics*, Cambridge University Press, Cambridge, 1993.
17. J. W. C. Johns, S. H. Priddle and D. A. Ramsay, *Discuss. Faraday Soc.*, 1963, **35**, 90-104.
18. J.-C. Loison, S. H. Kable, P. L. Houston and I. Burak, *J. Chem. Phys.*, 1991, **94**, 1796-1802.
19. J. Weiss, R. Schinke and V. Mandelshtam, *J. Chem. Phys.*, 2000, **113**, 4588-4597.
20. E. Renner, *Z. Phys.*, 1934, **92**, 172-193.
21. S. H. Kable, J.-C. Loison, P. L. Houston and I. Burak, *J. Chem. Phys.*, 1990, **92**, 6332-6333.
22. S. H. Kable, J.-C. Loison, D. W. Neyer, P. L. Houston, I. Burak and R. N. Dixon, *J. Phys. Chem.*, 1991, **95**, 8013-8018.
23. D. W. Neyer, S. H. Kable, J.-C. Loison, P. L. Houston, I. Burak and E. M. Goldfield, *J. Chem. Phys.*, 1992, **97**, 9036-9045.
24. E. M. Goldfield, S. K. Gray and L. B. Harding, *J. Chem. Phys.*, 1993, **99**, 5812-5827.
25. A. Loettgers, A. Untch, H.-M. Keller, R. Schinke, H.-J. Werner, C. Bauer and P. Rosmus, *J. Chem. Phys.*, 1997, **106**, 3186-3204.
26. S. Han, X. Zheng, S. Ndengué, Y. Song, R. Dawes, D. Xie, J. Zhang and H. Guo, *Sci. Adv.*, 2019, **5**, eaau0582.
27. S. Han, G. Sun, X. Zheng, Y. Song, R. Dawes, D. Xie, J. Zhang and H. Guo, *J. Phys. Chem. Lett.*, 2021, **12**, 6582-6588.
28. G. Amaral, K. Xu and J. Zhang, *J. Chem. Phys.*, 2001, **114**, 5164-5169.
29. W. Zhou, Y. Yuan, S. Chen and J. Zhang, *J. Chem. Phys.*, 2005, **123**, 054330.
30. G. Sun, W. Zhou, X. Zheng, Y. Qin, Y. Song, Y. Yuan and J. Zhang, *Mole. Phys.*, 2021, **119**, e1837974.
31. R. N. Zare, *Mole. Photochem.*, 1972, **4**, 1-37.
32. C. Petrongolo, *J. Chem. Phys.*, 1988, **89**, 1297-1308.
33. S. A. Ndengué, R. Dawes and H. Guo, *J. Chem. Phys.*, 2016, **144**, 244301.
34. L. Zhou, B. Jiang, D. Xie and H. Guo, *J. Phys. Chem. A*, 2013, **117**, 6940-6947.

35. J. Cullum and R. A. Willoughby, in *Large Scale Eigenvalue Problems*, eds. J. Cullum and R. A. Willoughby, Elsevier, 1986, pp. 193-240.
36. R. Chen and H. Guo, *J. Chem. Phys.*, 1996, **105**, 3569-3578.
37. H. Guo, *J. Chem. Phys.*, 1998, **108**, 2466-2472.
38. B. Jiang, D. Xie and H. Guo, *J. Chem. Phys.*, 2012, **136**, 034302.
39. L. Zhou, D. Xie and H. Guo, *J. Chem. Phys.*, 2015, **142**, 124317.
40. H. Tal-Ezer and R. Kosloff, *J. Chem. Phys.*, 1984, **81**, 3967-3971.

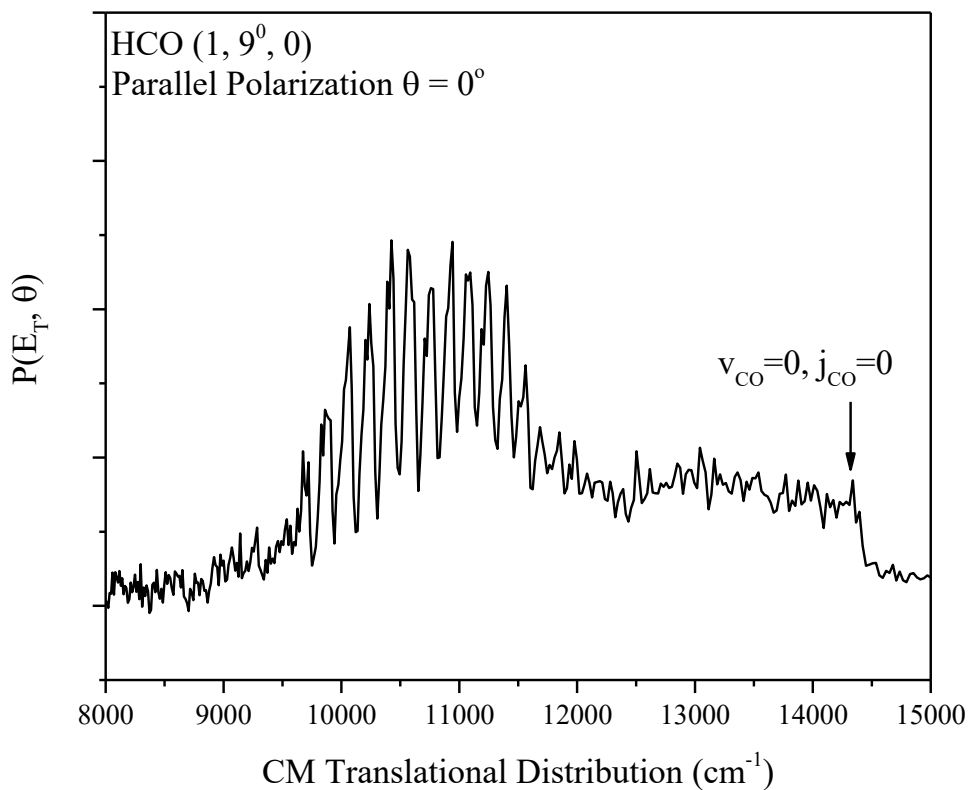


Figure 1. H + CO product CM translational energy distributions from the photodissociation of the HCO(\tilde{A}^2A'') (1, 9⁰, 0) state. The product translational energy of the rovibrational ground state ($v=0, j=0$) CO product is indicated by an arrow.

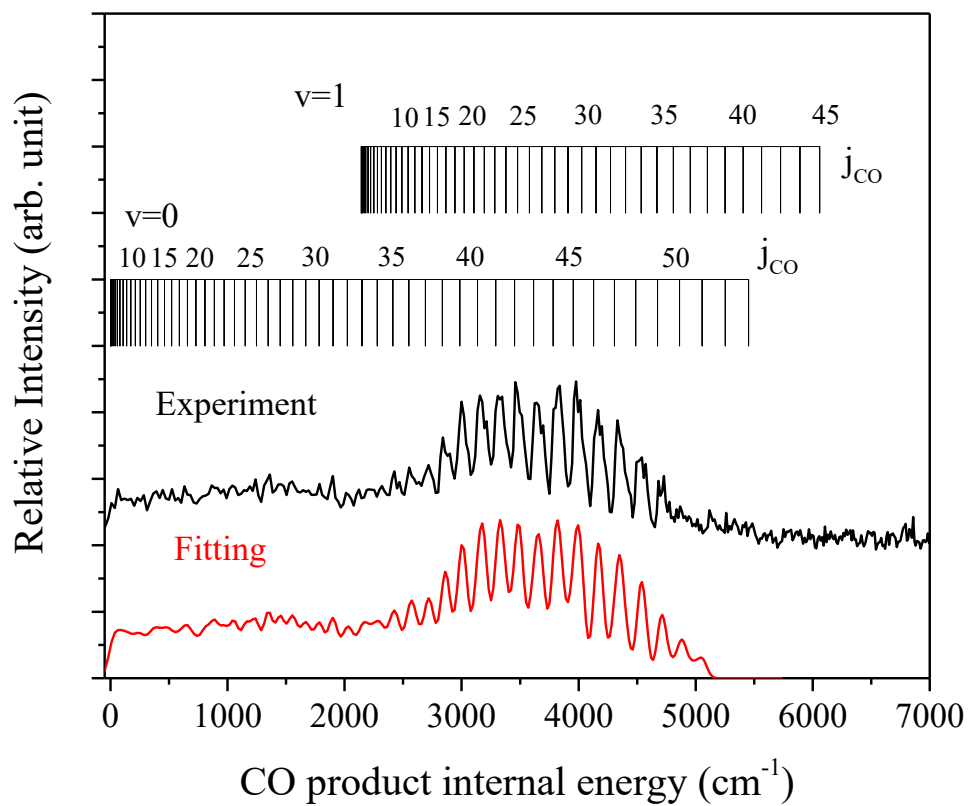


Figure 2. CO ($X^1\Sigma^+$, $v=0$ and 1) product internal energies and the fitting result from the photodissociation of the $\text{HCO}(\tilde{A}^2A'')$ ($1, 9^0, 0$) state.

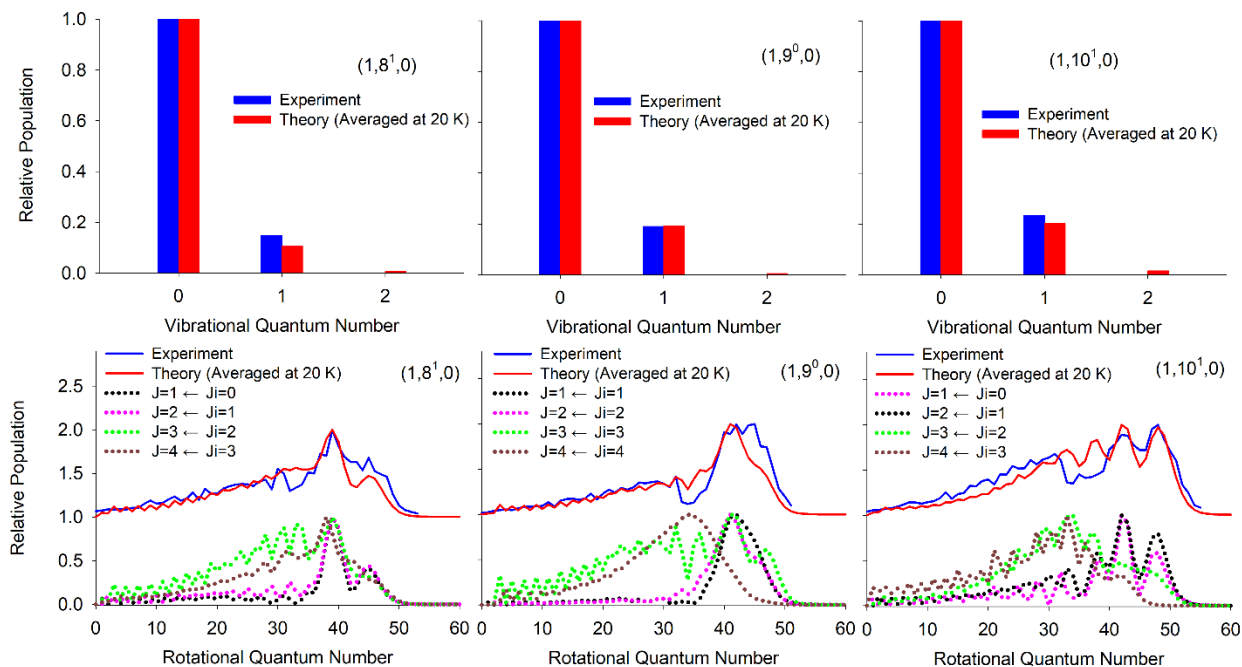


Figure 3. Top panel: comparison of the calculated and experimental vibrational distributions at energies of (from left to right) the $(1, 8^1, 0)$, $(1, 9^0, 0)$, and $(1, 10^1, 0)$ states of $\text{HCO}(\tilde{A}^2A'')$. Bottom panel: comparison of the calculated and experimental rotational distributions of $\text{CO}(v=0)$ at the same energies. Calculated distributions were averaged over all possible $J \leftarrow J_i$ transitions and some were selected are shown to display the trend. Note $J_i=1, 2, 3,$ and 4 refer to the $1_{01}, 2_{02}, 3_{03}$ and 4_{04} rotational states of $\text{HCO}(\tilde{X}^2A')$, respectively.

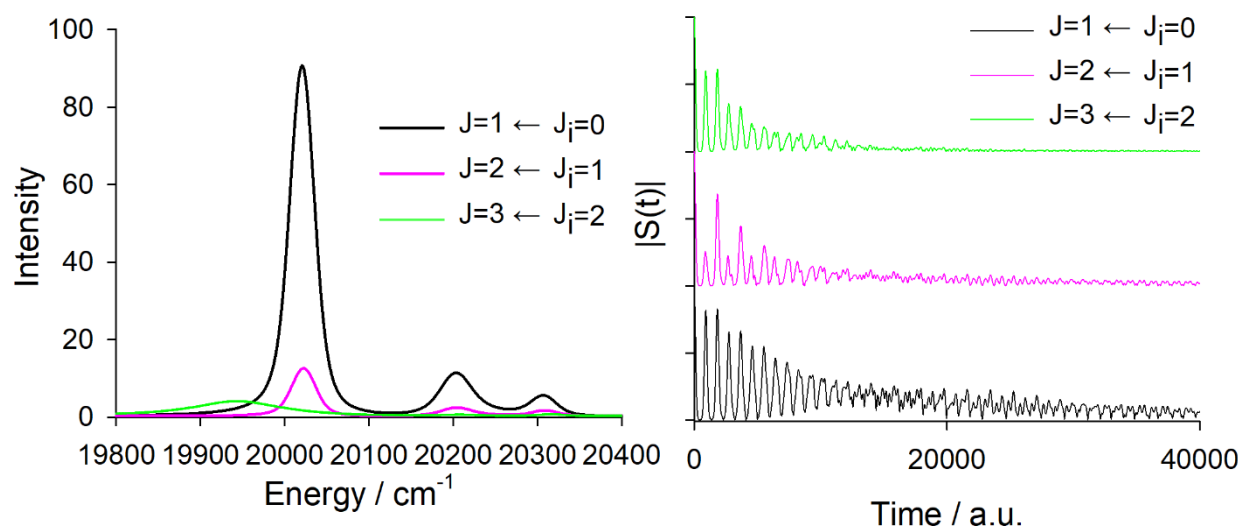


Figure 4. Calculated absorption spectra in the energy range of $(0, 14^1, 0)$, $(1, 10^1, 0)$ and $(0, 12^1, 1)$ from three different transitions. The excitation energy is placed at the energy of the $(1, 10^1, 0)$ state. The lifetime is compared through the autocorrelation function $|S(t)|$. Note $J_i=1, 2$, and 3 , refer to 1_{01} , 2_{02} and 3_{03} , and the shown transitions are the R branch. A similar figure for the Q branch can be found in a previous study.²⁷

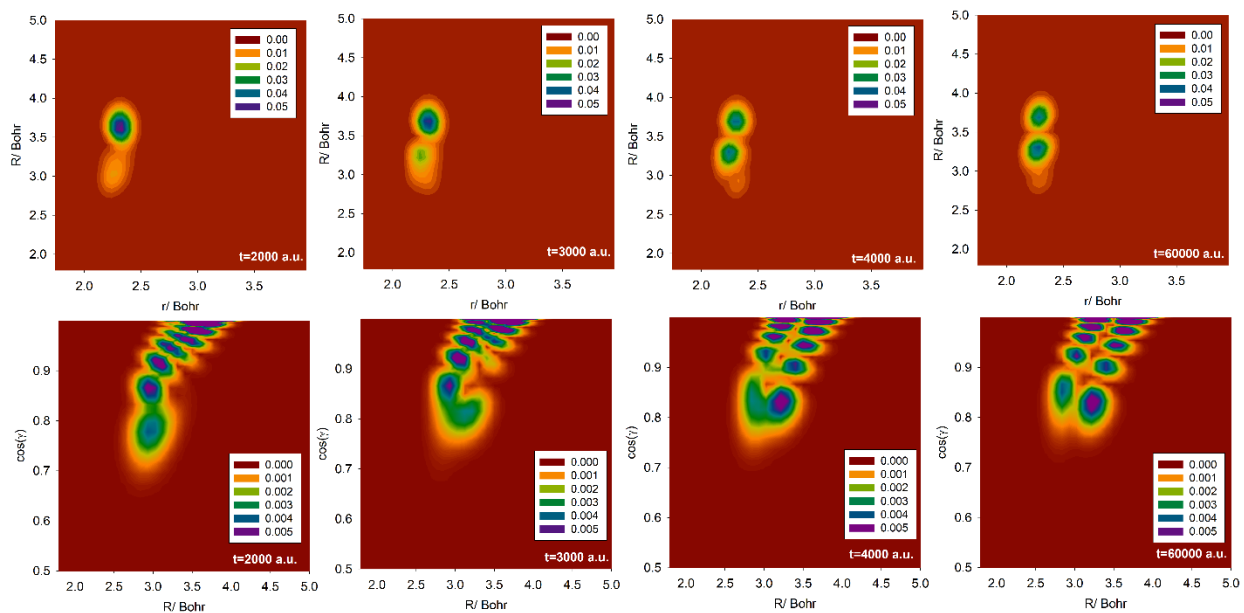


Figure 5. Time-dependent excited-state wave packet in the H-CO Jacobi coordinates (R, r, γ) .

The excitation energy is chosen at the energy of the $(1, 10^1, 0)$ state of $\text{HCO}(\tilde{A}^2 A'')$. The upper panels are densities integrated over r and the lower over γ .